HHS Public Access

Author manuscript

J Comp Neurol. Author manuscript; available in PMC 2019 December 15.

Published in final edited form as:

J Comp Neurol. 2018 December 15; 526(18): 2973–2983. doi:10.1002/cne.24503.

Phrenic motoneuron structural plasticity across models of diaphragm muscle paralysis

Carlos B. Mantilla[1,2,*], **Wen-Zhi Zhan**[2], **Heather M. Gransee**[1], **Y. S. Prakash**[1,2], and **Gary C. Sieck**[1,2]

[1]Depts. of Anesthesiology & Perioperative Medicine, Mayo Clinic, Rochester, MN 55905

[2]Depts. of Physiology & Biomedical Engineering, Mayo Clinic, Rochester, MN 55905

Abstract

Structural plasticity in motoneurons may be influenced by activation history and motoneuron-muscle fiber interactions. The goal of this study was to examine morphological adaptations of phrenic motoneurons following imposed motoneuron inactivity while controlling for diaphragm muscle inactivity. Well-characterized rat models were used including unilateral C2 spinal hemisection (SH; ipsilateral phrenic motoneurons and diaphragm muscle are inactive) and tetrodotoxin phrenic nerve blockade (TTX; ipsilateral diaphragm muscle is paralyzed while phrenic motoneuron activity is preserved). We hypothesized that inactivity of phrenic motoneurons would result in a decrease in motoneuron size, consistent with a homeostatic increase in excitability. Phrenic motoneurons were retrogradely labeled by ipsilateral diaphragm muscle injection of fluorescent dextrans or cholera toxin subunit B. Following 2 weeks of diaphragm muscle paralysis, morphological parameters of labeled ipsilateral phrenic motoneurons were assessed quantitatively using fluorescence confocal microscopy. Compared to controls, phrenic motoneuron somal volumes and surface areas decreased with SH, but increased with TTX. Total phrenic motoneuron surface area was unchanged by SH, but increased with TTX. Dendritic surface area was estimated from primary dendrite diameter using a power equation obtained from 3D reconstructed phrenic motoneurons. Estimated dendritic surface area was not significantly different between control and SH, but increased with TTX. Similarly, TTX significantly increased total phrenic motoneuron surface area. These results suggest that ipsilateral phrenic motoneuron morphological adaptations are consistent with a normalization of motoneuron excitability following prolonged alterations in motoneuron activity. Phrenic motoneuron structural plasticity is likely more dependent on motoneuron activity (or descending input) than muscle fiber activity.

Graphic abstract

Phrenic motoneuron morphology in rats was assessed quantitatively using confocal microscopy following unilateral diaphragm muscle paralysis induced by C2 spinal hemisection (SH) or tetrodotoxin phrenic nerve blockade (TTX). Ipsilateral motoneuron somal surface area decreased after SH and increased after TTX, indicating that structural plasticity does not depend on muscle inactivity.

[*]Correspondence to: Carlos B. Mantilla, M.D., Ph.D., MB 2-758 SMC, Mayo Clinic, Rochester, MN 55905, Tel: (507) 255-7481, Fax: (507) 255-7300, mantilla.carlos@mayo.edu.

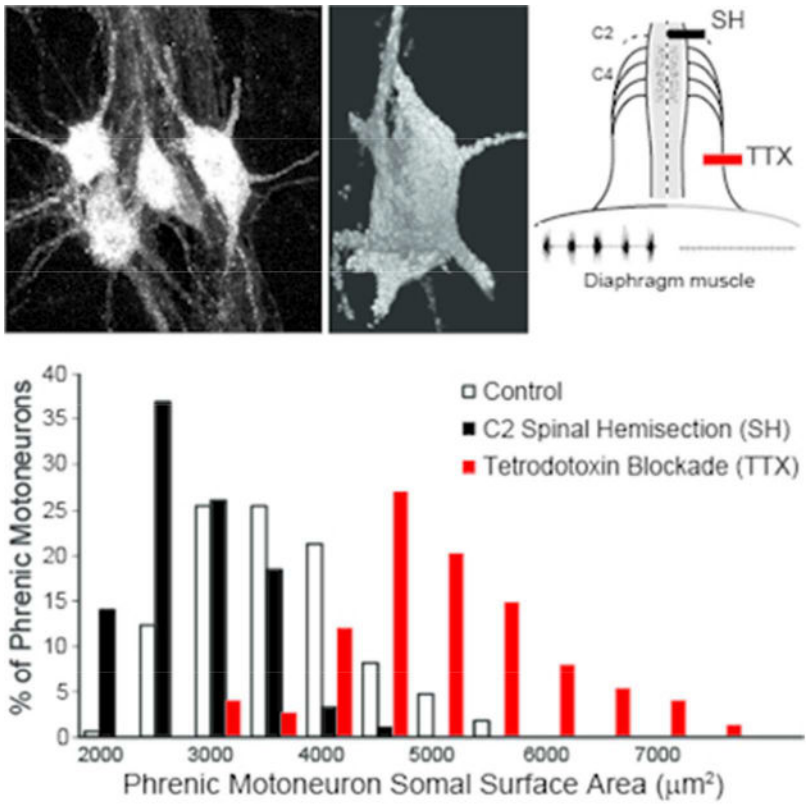

Keywords

Respiratory Muscles; Spinal Cord Injury; Tetrodotoxin; RRID:RGD_5508397; RRID:SCR_001775; RRID:SCR_005988

INTRODUCTION

Changes in neuronal activity, including inactivity, induce functional and structural plasticity in various systems (Bi and Poo, 2001; Segal and Andersen, 2000; Streeter and Baker-Herman, 2014). Examples of functional plasticity include both short and long term potentiation and depression in the hippocampus in response to altered activity, which have been attributed to changes in synaptic efficacy (Steward et al., 2001; Tomasulo et al., 1993; Tomasulo and Steward, 1996). Structural plasticity including synaptic remodeling is evident in hippocampal preparations after anoxic/hypoglycemic (Jourdain et al., 2002) or glutamate-induced excitotoxic injury (Goldin et al., 2001). In general, structural plasticity occurs over a longer time period and may involve not only synaptic remodeling but also changes in neuron morphology. Compared to the considerable literature on central and sensory neurons, very little is known about activity-dependent structural plasticity in motoneurons, especially as a result of motoneuron inactivity.

Phrenic motoneurons are highly active in sustaining ventilation. For example, the diaphragm muscle has a duty cycle of ~40% in contrast to the duty cycle of motoneurons innervating hindlimb muscles (~1–2% for soleus and ~15% for extensor digitorum longus muscle)

(Sieck, 1995; Sieck and Fournier, 1989; Sieck and Prakash, 1997). Thus, phrenic motoneurons appear well adapted for sustained activity. Accordingly, imposition of inactivity (e.g, cervical spinal cord injury or prolonged mechanical ventilation) may particularly affect phrenic motoneurons. There is currently a paucity of information regarding inactivity-induced phrenic motoneuron plasticity, especially regarding structural adaptations. In models of phrenic motoneuron inactivity, functional adaptations include partial recovery of motor function under increased ventilatory drive following incomplete spinal cord injury (Goshgarian et al., 1989; Hernandez-Torres et al., 2017; Mantilla et al., 2013a; Mantilla et al., 2013b; Martinez-Galvez et al., 2016; Nantwi and Goshgarian, 2001; O'Hara and Goshgarian, 1991) as well as long term potentiation following cervical deafferentation (Kinkead et al., 1998) and pharmacologically-imposed motoneuron inactivity (Streeter and Baker-Herman, 2014). Taken together, these data suggest that phrenic motoneuron inactivation results in adaptations that serve to restore phrenic motoneuron function. Based on Henneman's size principle (Henneman, 1957; Henneman et al., 1965), intrinsic excitability of neurons is dependent on membrane surface area (capacitance, resistance and rheobase) such that retraction of neuron size (somal and dendritic) leads to increased excitability. In the present study, we hypothesized that inactivity of phrenic motoneurons, induced by a C2 cervical spinal hemisection (SH), would result in a decrease in motoneuron size and since muscle paralysis also results from SH, to control for muscle inactivity *per se,* we performed additional experiments with tetrodotoxin (TTX) blockade of the phrenic nerve. TTX blockade causes unilateral diaphragm muscle paralysis without affecting the activity of phrenic motoneurons or interrupting axonal transport between the nerve and muscle.

METHODS

Adult male Sprague-Dawley rats (initial body weight ~300 g) were assigned randomly to the following groups: spinal hemisection (SH; n=5), sham spinal hemisection (SHAM-SH; n=3), tetrodotoxin-blockade of the phrenic nerve (TTX; n=5), sham TTX block (SHAM-TTX; n=2) and untreated control (n=4). Female rats were not included given expected differences in body size and possibly in dendritic arborization in this age group (Keil et al., 2017). All experimental procedures were approved by the Institutional Animal Care and Use Committee at Mayo Clinic, and in accordance with the American Physiological Society Animal Care Guidelines. For surgical procedures, animals were anesthetized by intramuscular injection of ketamine (60–90 mg/kg body weight) and xylazine (2.5–10 mg/kg), and administered antibiotics (Penicillin G) and analgesics (acetaminophen) for the first 5 days.

Spinal Hemisection.

Details of the SH surgical procedure have been previously published (Gransee et al., 2017; Gransee et al., 2013; 2015; Mantilla et al., 2007; Miyata et al., 1995; Prakash et al., 1999). Under sterile conditions, a bilateral dorsal C2 laminectomy was performed and the right half of the spinal cord was sectioned lateral to the dorsal fissure, thus transecting only the ventral and lateral funiculi, while preserving the dorsal funiculus on the side of SH. Ipsilateral (right) phrenic motoneuron inactivity following SH was verified by absence of

electroneurographic (ENG) activity, and paralysis of the ipsilateral hemidiaphragm was verified by the absence of electromyographic (EMG) activity at the terminal experiment by using pairs of electrode wires that were implanted into the midcostal diaphragm muscle, as previously described (Fig. 1) (Dow et al., 2006; Dow et al., 2009; Khurram et al., 2017; Mantilla et al., 2011; Trelease et al., 1982). In the SHAM-SH group, the spinal cord was exposed by cutting the dura but the cord was not sectioned.

TTX Blockade.

Details of this model have also been previously published (Mantilla et al., 2007; Mantilla and Sieck, 2009; Prakash et al., 1999; Zhan and Sieck, 1992). Animals were anesthetized and the right phrenic nerve was exposed in the neck. A Silastic cuff (OD 2 mm; ID 1.5 mm, 2 mm long) was placed around the phrenic nerve and sutured to surrounding muscles. A tunneled polyethylene cannula connected the cuff to a miniosmotic pump (OD 7 mm, 30 mm long; weight 1.1 g), which was subcutaneously implanted in the dorsum of the animal. The miniosmotic pump delivered 0.0125% TTX at a constant rate of 0.5 μ1/h over 2 weeks. In the SHAM-TTX group, the pump was filled with saline. The absence of ipsilateral diaphragm EMG activity at the terminal experiment confirmed paralysis of the ipsilateral hemidiaphragm (Fig. 1).

Phrenic Motoneuron Labeling.

Phrenic motoneurons were retrogradely labeled as previously described using intramuscular or intrapleural techniques (Fogarty et al., 2018; Mantilla et al., 2009; Prakash et al., 2000; Prakash et al., 1993; Zhan et al., 2000). For intramuscular injection, two days prior to the terminal experiment, animals were anesthetized, the right midcostal diaphragm muscle was exposed via a subcostal abdominal incision and injected with 5–10 μ1 of either 2% tetramethylrhodamine dextran (MW=3000 kD; ThermoFisher, Waltham, MA) or 1% cholera toxin subunit B (CTB; List Biologicals Labs, Inc., Campbell, CA) at each of 5 separate sites. Following the injections, the incision was closed and the animals recovered for 2 days. For intrapleural injection, Alexa Fluor 488-conjugated CTB (15 μl of a 0.2% solution, ThermoFisher) was administered ipsilaterally (Mantilla et al., 2009).

At the terminal experiment (2 weeks post-SH, TTX or SHAM surgery), animals were anesthetized and transcardially-perfused with heparinized saline followed by 4% paraformaldehyde in 0.1 M phosphate buffer (pH 7.4). The cervical spinal cord was then rapidly excised and post-fixed in 4% paraformaldehyde at 4°C overnight, followed by 25% sucrose in 0.1 M phosphate buffer for 24 h or more until sectioning. Coronal sections (100 μm thick) were cut on a cryostat (Reichert-Jung) and placed in phosphate buffer.

In a subset of animals injected with CTB, dendritic analyses were conducted using spinal cord sections that were incubated with 10% normal donkey serum in 0.1–1% Triton TBS, followed by anti-CTB (1:8,000; List Biologicals), biotinylated donkey anti-goat IgG (1:1,000; Jackson Immunoresearch, West Grove, PA) and then horseradish peroxidase-conjugated streptavidin (1:1000; Jackson Immunoresearch). Peroxidase was visualized using a glucose oxidase-imidazole-diaminobenzidine solution (Smithson et al., 1984), which yields a brown deposit in labeled neurons easily viewed under brightfield illumination. The

sections were washed in TBS, mounted on gel-subbed slides, dehydrated in graded alcohols, and coverslipped with DPX mounting media (Fluka, MilliporeSigma, St. Louis, MO).

In additional studies, the spinal cord was excised 72h after intrapleural tracer injection, fixed in 4% paraformaldehyde, and embedded in 2% agarose. Subsequently, 150 μm coronal sections of the spinal cord were cut using a Vibroslicer (Leica, Buffalo Grove, IL). Sections containing the ventral horn were placed on the bottom of a Sylgard (Dow Corning, Midland, MI)-lined dish and gently affixed with pins. The use of Alexa 488-CTB labeling of phrenic motoneurons aided in guiding the lucifer yellow (LY)-microelectrode through the membrane of superficially-located phrenic motoneurons within the lightly-fixed tissue (Obregon et al., 2009). Retrogradely-labeled phrenic motoneurons were visualized using an Olympus upright microscope equipped with a Photometrics Cascade CCD camera (Photometrics, Tucson, AZ) and injected using custom-fabricated micropipettes filled with 2% aqueous solution of LY (MilliporeSigma) in 0.5 mM lithium chloride (Obregon et al., 2009). Negative current pulses (100 ms, 1.0–1.5 nA, 3–4 Hz) were passed through the microelectrode with a Grass S88 stimulator (Natus Medical Inc, Pleasanton, CA.) (Ermilov et al., 2003; Ermilov et al., 2004). A 10–20 min injection of LY yielded complete filling of phrenic motoneurons, including dendritic trees. Spinal cord sections were then placed on a glass slide while preserving their orientation, dehydrated in graded alcohols, and coverslipped using DPX mounting media.

Phrenic Motoneuron Analyses.

Fluorescently labeled ipsilateral phrenic motoneurons (tetramethylrhodamine dextran or CTB) were visualized using a laser-scanning confocal system with an Olympus DApo x40 oil immersion lens (NA 1.3) and a step size of 1 μm. Images were analyzed using a multidimensional display, processing and measurement package (Analyze; AnalyzeDirect, Overland Park, KS). The procedures for phrenic motoneuron somal volume measurements have been described previously (Fogarty et al., 2018; Issa et al., 2010; Prakash et al., 2000; Prakash et al., 1993; 1994). Surface areas of motoneuron somata were estimated for a prolate spheroid by measuring the major and minor diameters (Fig. 2). The number of primary dendrites of each motoneuron was determined from 3D reconstructions, and dendritic diameter was measured from reformatted images orthogonal to the dendrites (measured at a distance of 15 μm from the somata) (Fogarty et al., 2018; Issa et al., 2010; Prakash et al., 2000; Zhan et al., 2000).

To render 3D representations of CTB-labeled ipsilateral phrenic motoneurons for dendritic measurements, a computer-controlled neuron tracing and morphometric system (NeuroLucida, MBF Bioscience, Williston, VT) was used. Labeled phrenic motoneurons were visualized on an Olympus BH-2 microscope with an Olympus DPlan x40 lens. The morphometric system was calibrated using a stage micrometer, and the Z-axis was controlled using a stepper motor, with a resolution of 0.1 μm. Dendrite length and branching were measured for intact phrenic motoneurons systematically sampled every 100 μm. Phrenic motoneurons were excluded if they were clearly damaged by the sectioning process. In each animal, at least 15 phrenic motoneurons were sampled.

LY-injected phrenic motoneurons were imaged on an Olympus confocal system with x60 oil immersion lens (NA 1.4) and a step size of 0.8 μm. A sequence of adjacent image stacks were captured for each phrenic motoneuron in order to image entire dendritic trees that extended beyond the field of view, ensuring that images on either side (top and bottom) of visible neuronal structures were included (Fig. 3). The step size was determined based on empirically calculated point spread function, and registration was verified empirically using fluorescently labeled microspheres (10 μm in diameter).

Eleven dendritic trees from LY-injected phrenic motoneurons (Fig. 3) were semi automatically segmented in Analyze and assigned to objects based on voxel intensities (Obregon et al., 2009; Prakash et al., 2000). Only phrenic motoneurons showing secondary order branching and greater were used for morphological analyses. The optimal correlation between dendritic tree surface area (A) and primary dendrite diameter (d_0) was obtained using the following power equation:

$$A = 1161.5 d_0^{1.03}$$

This equation was used to estimate the surface area of the dendritic tree from measurements of primary dendrite diameters.

Statistical Analyses.

Morphological parameters were compared across experimental groups using one-way ANOVA. When appropriate, post-hoc analyses were conducted using the Tukey-Kramer honestly significant difference test. Statistical significance was established at the $p<0.05$ level. Initial analysis revealed no significant difference across SHAM-SH, SHAM-TTX and control groups. Therefore, these groups were pooled in further statistical analyses and will be denoted as control from this point forward. All values presented are mean ± SE, unless otherwise stated.

RESULTS

Animal body weight increased by ~20% across all experimental groups over the 2 week experimental period. By the third day after SH, all animals displayed normal ambulation with only minor deficits in fine motor control. Both SH (n=5) and TTX (n=5) animals displayed altered movements of the rib cage and abdomen resulting from hemidiaphragm paralysis (Miyata et al., 1995; Prakash et al., 1999).

Verification of Surgical Procedures.

Histological examination of the SH spinal cords confirmed lesions restricted to the lateral and ventral funiculi. In TTX rats, there was no histological evidence of phrenic nerve damage at the site of the nerve cuff placement. Phrenic motoneuron inactivity following SH was verified by absence of ENG activity (Fig. 1). In contrast, ENG recordings of the phrenic nerve proximal to the TTX block showed persistent activity of phrenic motoneurons (Fig. 1). In all SH and TTX animals, ipsilateral diaphragm EMG activity was absent immediately

after surgery. SH animals were included in this study only if there was absence of ipsilateral diaphragm EMG activity at 14 days after surgery.

Phrenic Motoneuron Labeling.

In all groups, phrenic motoneurons were extensively labeled by both fluorescent dextrans and CTB (Fig. 2 and 4) and only ipsilateral to SH or TTX, forming a column located in the medial aspect of the ventral horn from the C3-C6 segments. There were no apparent differences in the spatial pattern of phrenic motoneuron labeling across the experimental groups, specifically TTX where partial denervation from potential TTX toxicity would have been a confounding factor.

The somata of labeled motoneurons appeared distinctly longer in the rostrocaudal axis, consistent with previous findings (Goshgarian and Rafols, 1981; Prakash et al., 2000; Prakash et al., 1993). Despite the extensive labeling, individual phrenic motoneurons could be easily discerned (Fig. 2), most likely because of discrete injections into the diaphragm muscle. Labeled motoneurons were often clustered in groups of 3–5 motoneurons. In such cases only a single phrenic motoneuron was sampled per cluster based on the completeness of the dendritic tree. Other sampled motoneurons were not included in clusters. This selection facilitated identification and tracking of the discrete dendritic trees of each identified motoneuron.

While extensive dendritic labeling was observed in all experimental groups using both fluorescent dextrans and CTB, more distal dendritic branches (on occasion, up to the fifth order) were often observed mostly with CTB (Fig. 2). There was extensive overlap in the dendritic fields of phrenic motoneurons, which additionally complicated the analyses of distal dendrites. The predominant orientation of dendrites was in the rostrocaudal axis, however dendritic branching in the mediolateral axis was also apparent. Dorsolateral projections were found, but these were not extensive. In most cases, dendritic branching was restricted to the ipsilateral spinal cord; however, some dendrites projected to the contralateral side. There were no apparent qualitative differences in the dendritic patterns between phrenic motoneurons of SH vs. control animals. However, compared to either group, phrenic motoneurons in the TTX group appeared to have greater dendritic arborization along the mediolateral axis. There were no apparent differences in the extent of contralateral projections across experimental groups. Overall, quantitative analyses were performed on 169, 92, and 74 phrenic motoneurons from control, SH and TTX groups, respectively. Only ipsilateral phrenic motoneurons whose cell body and primary dendrites were completely contained within the tissue section (displaying 5 or more primary dendrites) were included in analyses.

Phrenic Motoneuron Somal Dimensions.

The long ($F_{2,334} = 264$; $p < 0.001$) and short diameter ($F_{2,334} = 880$; $p < 0.001$) of labeled phrenic motoneurons was different across groups. The long diameter in the SH group (39 ± 1 μm) was significantly less than control (48 ± 1 μm), which was significantly less than the TTX group (79 ± 2 μm). The short diameter in the SH group (21 ± 1 μm) was significantly less than control (22 ± 1 μm), and the TTX group (19 ±1 μm) was significantly less than

control and SH. Typically, the long diameter of labeled phrenic motoneurons was approximately 2- to 4-fold greater than the short diameter, supporting the assumption of a prolate spheroidal shape (Prakash et al., 1993). Based on this assumption, and the diameter measurements, somal volume and surface area were estimated.

Phrenic motoneuron somal volume was different across groups (Fig. 5; $F_{2,334} = 116$; $p < 0.001$). In the SH group, phrenic motoneuron somal volume was significantly decreased (range: 5,523–13,729 μm^3) compared to control (range: 7,461–19,608 μm^3). In contrast, with TTX, somal volume was increased (range: 8,903–23,736 μm^3) compared to control as well as SH. Similarly, differences in somal surface area were evident across groups (Fig. 6; $F_{2,334} = 178$; $p < 0.001$). Somal surface area was also reduced in SH (range: 1,616–4,098 μm^2) compared to control (range: 1,981–5,476 μm^2), but increased in TTX (range: 2,723–7,740 μm^2). The distribution of phrenic motoneuron somal volumes and surface areas was determined using Z-scores based on the mean of each experimental group. In all 3 groups, somal volumes displayed a unimodal distribution, with the control group being similar to that observed in a previous study (Prakash et al., 2000). Compared to control, the distribution of somal volumes in SH animals was shifted to the left with an overall decrease in volume (Fig. 5). In contrast, in TTX animals, somal volume distribution was shifted to the right, with an overall increase in volume (Fig. 5). Similar shifts in the distribution of somal surface area were evident (Fig. 6).

Phrenic Motoneuron Dendritic Dimensions.

The number of primary dendritic branches and the primary dendrite diameter were not significantly different between phrenic motoneurons of control and SH animals (Table 1). Phrenic motoneurons from TTX animals had significantly more primary dendrites ($F_{2,334} = 6.03$; $p = 0.003$) as well as larger primary dendrite diameter ($F_{2,334} = 24.9$; $p < 0.001$) than control and SH animals.

Estimates of dendritic surface area based on primary dendrite diameter were developed using a sample of intracellularly labelled motoneurons from control rats. Eleven full dendritic arbors showing minor damage from sectioning were manually segmented and assigned to objects based on voxel intensities (Fig. 3). Dendritic branching ranged from 3rd to 7th order. The space occupied by the neuron was arbitrarily divided into several regions with the landmarks common to all or at least to the adjacent regions in order to capture the entire visible dendritic arbor. For each region a stack of images was separately collected, volume reconstructed and merged, as described previously (Ermilov et al., 2000). Dendritic branches were widely dispersed within the depth of spinal cord, and only the volume rendered images of dendritic trees ($n = 11$) that were entirely within the field of view and had no visible damages were selected for 3D morphometry, based on a previous study (Obregon et al., 2009). A power model resulted in the best fit correlation between dendritic tree surface area and primary dendrite diameter ($r^2 = 0.880$).

Dendritic surface area was estimated from primary dendrite diameter of labeled phrenic motoneurons using this equation. Estimated dendritic surface area was not significantly different between control and SH, but increased with TTX (Fig. 7; $F_{2,334} = 13.6$; $p < 0.001$). The distribution of estimated dendritic surface area was skewed to the right with TTX.

Similarly, total phrenic motoneuron surface area was not significantly different between control and SH, but increased with TTX (Table 1; $F_{2,334} = 18.3$; $p < 0.001$).

In addition to the estimated surface area, the total area across which dendrites from an individual phrenic motoneuron (receptive area) was calculated from a polygon connecting the ends of the most distal dendrites visualized in CTB-labeled phrenic motoneurons. In these measurements, dendrites were found to expand to similar extents as control following SH and TTX ($p = 0.072$; Table 1). However, the average dendritic length was increased after TTX compared to SH ($p = 0.015$; Table 1).

DISCUSSION

The present study examined phrenic motoneuron morphology in a model of phrenic motoneuron inactivity induced by SH, and compared these findings to those induced by diaphragm muscle inactivity in the absence of phrenic motoneuron inactivity (utilizing a model of unilateral TTX block of the phrenic nerve). Ipsilateral phrenic motoneuron inactivity resulted in decreased somal dimensions but unchanged dendritic dimension, supporting our hypothesis and consistent with an overall increase excitability in the phrenic motor pool. In contrast, diaphragm muscle paralysis without inactivity of phrenic motoneurons resulted in increased phrenic motoneuron size. Our data suggest that morphological adaptations of phrenic motoneurons to inactivity are likely dependent on intrinsic motoneuron properties and/or altered descending synaptic input (not on target muscle activity). These changes likely occur in order to maintain or restore intrinsic excitability of the phrenic motoneuron pool.

Adaptations of Phrenic Motoneurons to SH and TTX

Although diaphragm muscle paralysis was evident in the SH and TTX models, phrenic motoneurons were inactive in SH animals, while phrenic motoneuron activity was present in the TTX group. In fact, in previous studies (Miyata et al., 1995; Zhan et al., 1997), we found that TTX increased integrated phrenic nerve activity by ~50%; however, whether this increase is maintained for the 2 week survival period is not known. In other studies where diaphragm paralysis is induced by unilateral denervation (Gill et al., 2015; Khurram et al., 2017), EMG activity in the intact hemidiaphragm increases. Regardless, SH is associated with concordant inhibition of phrenic motoneuron and diaphragm muscle activity, while TTX is associated with discordance between motoneuron and muscle activities.

The present study found that SH and TTX differed in the pattern of somal and dendritic alterations. In addition, adaptations in dendritic arborization did not match changes in somal volume and surface areas. Ipsilateral motoneuron somal volumes and surface areas decreased with SH, but increased with TTX. Although dendritic receptive fields were similar with both SH and TTX, the mean branch length was significantly increased following TTX compared to SH. Following SH, there was no change in estimated total surface area, whereas total surface area increased following TTX. However, given that dendritic and total surface area measurements are indeed estimates, they must be interpreted with caution. Regardless, the somal vs. dendritic changes observed with SH are consistent with our hypothesis that phrenic motoneuron adaptations to SH serve to increase excitability, which may contribute

to spontaneous restoration of function (Gransee et al., 2017; Gransee et al., 2013; 2015; Hernandez-Torres et al., 2017; Mantilla et al., 2012; Mantilla et al., 2013a; 2017; Mantilla et al., 2014; Mantilla et al., 2013b; Martinez-Galvez et al., 2016). The present study specifically selected animals not displaying recovery of rhythmic diaphragm EMG activity post-SH in order to avoid the confounding effects of restored function, but the underlying mechanisms are expected to be similar in animals displaying recovery vs. those not.

Although muscle inactivity with TTX was persistent for the duration of the study (paralysis was verified at the terminal experiment), it is not possible to ascertain the level of change (if any) in motoneuron activity (at the cell soma). In the absence of direct measurements of motoneuron activity at the terminal experiment (precluded by sampling issues of single motoneuron recordings), we cannot incorporate the morphological changes seen after TTX with changes in motoneuron activity. Based on recent studies from our group examining changes in contralateral diaphragm EMG activity following denervation (Gill et al., 2015; Khurram et al., 2017), there is a suggestion that descending inputs to phrenic motoneurons increase ~50%, but it is not possible to ascertain whether there are motor unit type differences in activation levels in these experiments. It is likely that phrenic motoneuron cell bodies experience greater drive two weeks after TTX, resulting in increased somal volume and surface area, as well as increased dendritic surface area. It is expected that with the TTX phrenic nerve blockade conduction along phrenic afferents is also blocked. However, activity of other afferents relevant to respiratory behaviors (e.g., chest wall or airway afferents) is expected to be unimpaired, although could be affected by changes in the respiratory pattern. Although this is possible, extensive experience in the SH or unilateral denervation models documents minimal changes in respiratory rate, tidal volume or transdiaphragmatic pressure during ventilatory behaviors, and no change in arterial blood gases (Gill et al., 2015; Gransee et al., 2017; Gransee et al., 2013; 2015; Hernandez-Torres et al., 2017; Khurram et al., 2017; Mantilla et al., 2013a; 2017).

There is currently no published information on the effects of inactivation due to SH on gross morphological changes of phrenic motoneurons. However, several studies have demonstrated significant ultrastructural changes in the cervical spinal cord following SH (Goshgarian et al., 1989; Hadley et al., 1999), including increased number of “double synapses” and increased length of dendro-dendritic appositions. These changes, which are more prominent with time, are unlikely to be induced by the SH itself since cold block of descending cervical drive also induces similar changes (Castro-Moure and Goshgarian, 1997). Taken together, these results support ongoing plasticity that aims to maintain or restore excitability of the phrenic motoneuron pool.

Although phrenic motoneuron dendritic arborization is primarily limited to the ipsilateral spinal cord (Lindsay et al., 1991), a previous study suggested there are occasional contralateral projections of phrenic motoneurons (Prakash et al., 2000). These dendritic projections may allow for phrenic motoneuron activation from the contralateral side, and may be especially important following weeks or months of SH in conjunction with any increased (or previously ineffective) contralateral supraspinal axonal input. In the present study, we found only occasional contralateral dendritic projections in both control and SH animals. Since the overall span of dendritic projections did not change significantly with SH,

it is likely that axonal decussations from intact contralateral (descending) projections play a more important role in the spontaneous recovery of ipsilateral diaphragm activity following SH (Mantilla and Sieck, 2003).

Phrenic Motoneuron Morphology

As described in previous studies including our own (Fogarty et al., 2018; Furicchia and Goshgarian, 1987; Goshgarian and Rafols, 1981; Issa et al., 2010; Prakash et al., 2000), characteristic features of phrenic motoneurons were observed in the present study, including rostrocaudal phrenic motoneuron clustering with preferred rostrocaudal and mediolateral dendritic orientations. This organization may act to integrate activity of phrenic motoneurons during the respiratory cycle, as well as facilitate interactions between phrenic motoneurons and adjacent motoneurons responsible for controlling accessory respiratory muscles (Scheibel and Scheibel, 1970; 1971). Afferent input from the brainstem has also been shown to follow the somatic and dendritic distribution of phrenic motoneurons (Ellenberger and Feldman, 1988; Ellenberger et al., 1990; Furicchia and Goshgarian, 1987; Wu et al., 2017).

In the present study, we integrated 3D confocal microscopy and dendritic modeling to determine changes in ipsilateral phrenic motoneuron morphology. This integrated approach significantly reduced the analytical burden created by the large volumes of 3D confocal image data. Furthermore, the phrenic motor nucleus spans ~1 cm along the spinal cord making it virtually impossible to create 3D sets of image data of sufficient resolution for detailed analysis of neuronal morphometry. A shape-based stereological technique was used to estimate phrenic motoneuron somal volumes and surface areas. We (Issa et al., 2010; Prakash et al., 1993) and others (Cameron and Fang, 1989; Cullheim et al., 1987a; Ulfhake and Cullheim, 1988) have previously reported that rat phrenic motoneurons can be largely represented by a prolate spheroidal shape. Furthermore, volume and area estimates assuming such geometry are <10% different from actual 3D confocal measurements (Prakash et al., 1993). Thus, the stereological approach significantly reduced the burden of analysis without biasing or altering the results.

Given the complex and extensive dendritic arborization of phrenic motoneurons, it was not possible to perform detailed and complete dendritic analyses from 3D confocal images, especially since only sections of spinal cord were imaged. Commonly employed techniques are based on retrograde labeling of specific motoneuron pools by intramuscular or intraneural injection (Boulenguez et al., 2007; Gordon and Richmond, 1990; Issa et al., 2010; Prakash et al., 2000; Yates et al., 1999; Zhan et al., 2000). The method of intrapleural injection allows specific labeling of phrenic motoneurons and permits near complete labeling of the entire motoneuron pool across developmental ages (Mantilla et al., 2009). However, filling of distal dendrites with any of these retrograde techniques is usually limited, regardless of fluorescent dye or peroxidase selection. In this study, we combined labeling of phrenic motoneurons via intrapleural injection with Alexa Fluor 488-conjugated CTB with intracellular injection of LY into these visually identified neurons in lightly fixed-spinal cord slices (C3-C6) (Obregon et al., 2009). This combined approach allows sampling of a relatively large number of motoneurons per animal and detailed three-dimensional

reconstruction of the dendritic tree of phrenic motoneurons from confocal slices. The combination of these labeling and imaging techniques considerably improved image quality and allowed reliable 3D visualization and direct morphometry of the identified phrenic motoneurons with an entire extension of their visible dendritic trees.

Accordingly, analysis of dendritic arborization was performed based on the novel model derived using 3D reconstructions of intracellularly-filled adult rat phrenic motoneurons (Obregon et al., 2009), without morphological assumptions that are used in dendritic models such as those developed by Burke et al. (Burke et al., 1992). For this calculation, dendritic surface area was estimated from primary dendrite diameter (which was reliably measured from the confocal images with <10% error). The reliability of this technique is underlined by the consistency of our estimates of dendritic surface area in control phrenic motoneurons with those previously reported by other investigators for α-motoneurons, including phrenic motoneurons (Cameron et al., 1985; Cameron et al., 1991) and hindlimb motoneurons (Cullheim et al., 1987a; b). In addition, an estimate of dendritic receptive field was obtained based on visible extent of dendritic branching.

Mechanisms Underlying Phrenic Motoneuron Adaptations

One mechanism that may mediate neuronal adaptations to altered activity is the role of trophic factors. Such trophic factors may be muscle-derived or neuron-derived, with both local (autocrine) and distant targets. Furthermore, the specific production of trophic factors or the localization of their receptors may dictate motor unit specificity of the response to trophic factors. Expression of neurotrophic factors such as ciliary neurotrophic factor, brain-derived neurotrophic factor, neurotrophin-3 and neurotrophin-4 change following lumbar spinal cord injury (Bennett et al., 1999; Bregman et al., 1997; Ikeda et al., 2001; Mantilla and Sieck, 2008; Oyesiku et al., 1997; Satake et al., 2000; Widenfalk et al., 2001). However, an important distinction with regard to limb muscles, compared to the diaphragm muscle, is whether spinal transection actually produces hindlimb motoneuron inactivation since the pattern generators are located in the spinal cord (rather than the brainstem as for phrenic motoneurons). In our study, SH clearly inactivated phrenic motoneurons. Recent studies from our laboratory support the role of neurotrophic factors acting on phrenic motoneurons in neuroplasticity underlying recovery of rhythmic diaphragm activity after SH (Gransee et al., 2013; 2015; Hernandez-Torres et al., 2017; Mantilla et al., 2013a; Mantilla et al., 2014; Martinez-Galvez et al., 2016). Future studies could determine whether SH and TTX nerve blockade induce differential expression of neurotrophic factors in phrenic motoneurons to elucidate underlying, intrinsic motoneuron adaptations to inactivity. A previous study comparing SH and TTX induced adaptations at the neuromuscular junction suggested indeed that the predominant changes occurred at the motoneuron axon terminal (Mantilla et al., 2007).

In both SH and TTX models, the potential for muscle-derived neurotrophic influence likely remained intact since axonal transport was unaffected (Miyata et al., 1995; Zhan and Sieck, 1992). However, possible changes in the expression of muscle-derived trophic factors (Dohrmann et al., 1986; Funakoshi et al., 1995; Griesbeck et al., 1995; Henderson et al., 1994) have not been examined following either SH or TTX nerve blockade. Furthermore,

the release of trophic factors may be constitutive and may reflect motor unit type differences. The results of the present study are suggestive of such motor unit-specific responses in phrenic motoneuron morphology.

Acknowledgments:

This research was supported by NIH grant HL096750.

REFERENCES

Bennett AD, Taglialatela G, Perez-Polo R, Hulsebosch CE. 1999 NGF levels decrease in the spinal cord and dorsal root ganglion after spinal hemisection. Neuroreport 10:889–893. [PubMed: 10208566]

Bi G, Poo M. 2001 Synaptic modification by correlated activity: Hebb's postulate revisited. Annual Review Of Neuroscience 24:139–166.

Boulenguez P, Gestreau C, Vinit S, Stamegna JC, Kastner A, Gauthier P. 2007 Specific and artifactual labeling in the rat spinal cord and medulla after injection of monosynaptic retrograde tracers into the diaphragm. Neurosci Lett 417:206–211. [PubMed: 17412505]

Bregman BS, McAtee M, Dai HN, Kuhn PL. 1997 Neurotrophic factors increase axonal growth after spinal cord injury and transplantation in the adult rat. Exp Neurol 148:475–494. [PubMed: 9417827]

Burke RE, Marks WB, Ulfhake B. 1992 A parsimonious description of motoneuron dendritic morphology using computer simulation. J Neurosci 12:2403–2416. [PubMed: 1607948]

Cameron WE, Averill DB, Berger AJ. 1985 Quantitative analysis of the dendrites of cat phrenic motoneurons stained intracellularly with horseradish peroxidase. J Comp Neurol 230:91–101.

Cameron WE, Fang H. 1989 Morphology of developing motoneurons innervating the medial gastrocnemius of the cat. Dev Brain Res 49:253–263. [PubMed: 2805334]

Cameron WE, He F, Kalipatnapu P, Jodkowski JS, Guthrie RD. 1991 Morphometric analysis of phrenic motoneurons in the cat during postnatal development. J Comp Neurol 314:763–776. [PubMed: 1816274]

Castro-Moure F, Goshgarian HG. 1997 Morphological plasticity induced in the phrenic nucleus following cervical cold block of descending respiratory drive. Exp Neurol 147:299–310. [PubMed: 9344555]

Cullheim S, Fleshman JW, Glenn LL, Burke RE. 1987a Membrane area and dendritic structure in type-identified triceps surae alpha motoneurons. J Comp Neurol 255:68–81. [PubMed: 3819010]

Cullheim S, Fleshman JW, Glenn LL, Burke RE. 1987b Three-dimensional architecture of dendritic trees in type-identified alpha-motoneurons. J Comp Neurol 255:82–96. [PubMed: 3819011]

Dohrmann U, Edgar D, Sendtner M, Thoenen H. 1986 Muscle derived factors that support and promote fiber outgrowth from embryonic chick spinal motor neurons in culture. Developmental Biology 118:209–221. [PubMed: 3770299]

Dow DE, Mantilla CB, Zhan WZ, Sieck GC. 2006 EMG-based detection of inspiration in the rat diaphragm muscle. Conf Proc IEEE Eng Med Biol Soc 1: 1204–1207. [PubMed: 17946030]

Dow DE, Zhan WZ, Sieck GC, Mantilla CB. 2009 Correlation of respiratory activity of contralateral diaphragm muscles for evaluation of recovery following hemiparesis. Conf Proc IEEE Eng Med Biol Soc 1:404–407.

Ellenberger HH, Feldman JL. 1988 Monosynaptic transmission of respiratory drive to phrenic motoneurons from brainstem bulbospinal neurons in rats. J Comp Neurol 269:47–57. [PubMed: 3361003]

Ellenberger HH, Vera PL, Haselton JR, Haselton CL, Schneiderman N. 1990 Brainstem projections to the phrenic nucleus: an anterograde and retrograde HRP study in the rabbit. Brain Res Bull 24:163–174. [PubMed: 1691045]

Ermilov LG, Miller SM, Schmalz PF, Hanani M, Lennon VA, Szurszewski JH. 2003 Morphological characteristics and immunohistochemical detection of nicotinic acetylcholine receptors on

intestinofugal afferent neurones in guinea-pig colon. Neurogastroenterol Motil 15:289–298. [PubMed: 12787338]

Ermilov LG, Miller SM, Schmalz PF, Hanani M, Szurszewski JH. 2000 The three-dimensional structure of neurons in the guinea pig inferior mesenteric and pelvic hypogastric ganglia. Auton Neurosci 83:116–126. [PubMed: 11593762]

Ermilov LG, Schmalz PF, Miller SM, Szurszewski JH. 2004 PACAP modulation of the colon inferior mesenteric ganglion reflex in the guinea pig. J Physiol 560:231–247. [PubMed: 15284351]

Fogarty MJ, Omar TS, Zhan WZ, Mantilla CB, Sieck GC. 2018 Phrenic Motor Neuron Loss in Aged Rats. J Neurophysiol 119:1852–1862. [PubMed: 29412773]

Funakoshi H, Belluardo N, Arenasa E, Yamamoto Y, Casabona A, Persson H, Ibanez CF. 1995 Muscle-derived neurotrophin-4 as an activity-dependent trophic signal for adult motor neurons. Science 268:1495–1499. [PubMed: 7770776]

Furicchia FV, Goshgarian HG. 1987 Dendritic organization of phrenic motoneurons in the adult rat. Exp Neurol 96:621–634. [PubMed: 3446220]

Gill LC, Mantilla CB, Sieck GC. 2015 Impact of unilateral denervation on transdiaphragmatic pressure. Respir Physiol Neurobiol 210:14–21. [PubMed: 25641347]

Goldin M, Segal M, Avignone E. 2001 Functional plasticity triggers formation and pruning of dendritic spines in cultured hippocampal networks. J Neurosci 21:186–193. [PubMed: 11150335]

Gordon DC, Richmond FJ. 1990 Topography in the phrenic motoneuron nucleus demonstrated by retrograde multiple-labelling techniques. J Comp Neurol 292:424–434. [PubMed: 2341610]

Goshgarian HG, Rafols JA. 1981 The phrenic nucleus of the albino rat: a correlative HRP and Golgi study. J Comp Neurol 201:441–456. [PubMed: 7276259]

Goshgarian HG, Yu XJ, Rafols JA. 1989 Neuronal and glial changes in the rat phrenic nucleus occurring within hours after spinal cord injury. J Comp Neurol 284:519–533. [PubMed: 2768550]

Gransee HM, Gonzalez Porras MA, Zhan WZ, Sieck GC, Mantilla CB. 2017 Motoneuron glutamatergic receptor expression following recovery from cervical spinal hemisection. J Comp Neurol 525:1192–1205. [PubMed: 27650492]

Gransee HM, Zhan WZ, Sieck GC, Mantilla CB. 2013 Targeted Delivery of TrkB Receptor to Phrenic Motoneurons Enhances Functional Recovery of Rhythmic Phrenic Activity after Cervical Spinal Hemisection. PloS one 8:e64755. [PubMed: 23724091]

Gransee HM, Zhan WZ, Sieck GC, Mantilla CB. 2015 Localized Delivery of Brain-Derived Neurotrophic Factor-Expressing Mesenchymal Stem Cells Enhances Functional Recovery following Cervical Spinal Cord Injury. J Neurotrauma 32:185–193. [PubMed: 25093762]

Griesbeck O, Parsadanian AS, Sendtner M, Thoenen H. 1995 Expression of neurotrophins in skeletal muscle: quantitative comparison and significance for motoneuron survival and maintenance of function. J Neurosci Res 42:21–33. [PubMed: 8531223]

Hadley SD, Walker PD, Goshgarian HG. 1999 Effects of serotonin inhibition on neuronal and astrocyte plasticity in the phrenic nucleus 4 h following C2 spinal cord hemisection. Exp Neurol 160:433–445. [PubMed: 10619560]

Henderson CE, Phillips HS, Pollack RA, Davies AM, Lemeulle C, Armanini M, Simpson LC, Moffet B, Vandlen RA, Koliatsos VE, Rosenthal A. 1994 GDNF: A potent survival factor for motoneurons present in peripheral nerve and muscle. Science 266:1062–1064. [PubMed: 7973664]

Henneman E 1957 Relation between size of neurons and their susceptibility to discharge. Science 126:1345–1346. [PubMed: 13495469]

Henneman E, Somjen G, Carpenter DO. 1965 Functional significance of cell size in spinal motoneurons. J Neurophysiol 28:560–580. [PubMed: 14328454]

Hernandez-Torres V, Gransee HM, Mantilla CB, Wang Y, Zhan WZ, Sieck GC. 2017 BDNF effects on functional recovery across motor behaviors after cervical spinal cord injury. J Neurophysiol 117:537–544. [PubMed: 27832605]

Ikeda O, Murakami M, Ino H, Yamazaki M, Nemoto T, Koda M, Nakayama C, Moriya H. 2001 Acute up-regulation of brain-derived neurotrophic factor expression resulting from experimentally induced injury in the rat spinal cord. Acta Neuropathol (Berl) 102:239–245. [PubMed: 11585248]

Issa AN, Zhan WZ, Sieck G, Mantilla CB. 2010 Neuregulin-1 at synapses on phrenic motoneurons. J Comp Neurol 518:4213–4225. [PubMed: 20878784]

Jourdain P, Nikonenko I, Alberi S, Muller D. 2002 Remodeling of hippocampal synaptic networks by a brief anoxia-hypoglycemia. J Neurosci 22:3108–3116. [PubMed: 11943814]

Keil KP, Sethi S, Wilson MD, Chen H, Lein PJ. 2017 In vivo and in vitro sex differences in the dendritic morphology of developing murine hippocampal and cortical neurons. Sci Rep 7:8486. [PubMed: 28814778]

Khurram OU, Sieck GC, Mantilla CB. 2017 Compensatory effects following unilateral diaphragm paralysis. Respir Physiol Neurobiol 246:39–46. [PubMed: 28790008]

Kinkead R, Zhan WZ, Prakash YS, Bach KB, Sieck GC, Mitchell GS. 1998 Cervical dorsal rhizotomy enhances serotonergic innervation of phrenic motoneurons and serotonin dependent long-term facilitation of respiratory motor output in rats. J Neurosci 18:8436–8443. [PubMed: 9763486]

Lindsay AD, Greer JJ, Feldman JL. 1991 Phrenic motoneuron morphology in the neonatal rat. J Comp Neurol 308:169–179. [PubMed: 1716267]

Mantilla CB, Bailey JP, Zhan WZ, Sieck GC. 2012 Phrenic motoneuron expression of serotonergic and glutamatergic receptors following upper cervical spinal cord injury. Exp Neurol 234:191–199. [PubMed: 22227062]

Mantilla CB, Gransee HM, Zhan WZ, Sieck GC. 2013a Motoneuron BDNF/TrkB signaling enhances functional recovery after cervical spinal cord injury. Exp Neurol 247C:101–109.

Mantilla CB, Gransee HM, Zhan WZ, Sieck GC. 2017 Impact of glutamatergic and serotonergic neurotransmission on diaphragm muscle activity after cervical spinal hemisection. J Neurophysiol 118:1732–1738. [PubMed: 28659464]

Mantilla CB, Greising SM, Stowe JM, Zhan WZ, Sieck GC. 2014 TrkB Kinase Activity is Critical for Recovery of Respiratory Function after Cervical Spinal Cord Hemisection. Exp Neurol 261:190–195. [PubMed: 24910201]

Mantilla CB, Greising SM, Zhan WZ, Seven YB, Sieck GC. 2013b Prolonged C2 spinal hemisection-induced inactivity reduces diaphragm muscle specific force with modest, selective atrophy of type IIx and/or IIb fibers. J Appl Physiol 114:380–386. [PubMed: 23195635]

Mantilla CB, Rowley KL, Zhan WZ, Fahim MA, Sieck GC. 2007 Synaptic vesicle pools at diaphragm neuromuscular junctions vary with motoneuron soma, not axon terminal, inactivity. Neuroscience 146:178–189. [PubMed: 17346898]

Mantilla CB, Seven YB, Hurtado-Palomino JN, Zhan WZ, Sieck GC. 2011 Chronic assessment of diaphragm muscle EMG activity across motor behaviors. Respir Physiol Neurobiol 177:176–182. [PubMed: 21414423]

Mantilla CB, Sieck GC. 2003 Invited Review: Mechanisms underlying motor unit plasticity in the respiratory system. J Appl Physiol 94:1230–1241. [PubMed: 12571144]

Mantilla CB, Sieck GC. 2008 Trophic factor expression in phrenic motor neurons. Respir Physiol Neurobiol 164:252–262. [PubMed: 18708170]

Mantilla CB, Sieck GC. 2009 Neuromuscular adaptations to respiratory muscle inactivity. Respir Physiol Neurobiol 169:133–140. [PubMed: 19744580]

Mantilla CB, Zhan WZ, Sieck GC. 2009 Retrograde labeling of phrenic motoneurons by intrapleural injection. J Neurosci Methods 182:244–249. [PubMed: 19559048]

Martinez-Galvez G, Zambrano JM, Diaz Soto JC, Zhan WZ, Gransee HM, Sieck GC, Mantilla CB. 2016 TrkB gene therapy by adeno-associated virus enhances recovery after cervical spinal cord injury. Exp Neurol 276:31–40. [PubMed: 26607912]

Miyata H, Zhan WZ, Prakash YS, Sieck GC. 1995 Myoneural interactions affect diaphragm muscle adaptations to inactivity. J Appl Physiol 79:1640–1649. [PubMed: 8594024]

Nantwi KD, Goshgarian HG. 2001 Alkylxanthine-induced recovery of respiratory function following cervical spinal cord injury in adult rats. Exp Neurol 168:123–134. [PubMed: 11170727]

O'Hara TEJ, Goshgarian HG. 1991 Quantitative assessment of phrenic nerve functional recovery mediated by the crossed phrenic reflex at various time intervals after spinal cord injury. Exp Neurol 111:244–250. [PubMed: 1989900]

Obregon G, Ermilov LG, Zhan WZ, Sieck GC, Mantilla CB. 2009 Modeling dendritic arborization based on 3D-reconstructions of adult rat phrenic motoneurons. Revista Ingenieria Biomedica 3:47–54.

Oyesiku NM, Wilcox JN, Wigston DJ. 1997 Changes in expression of ciliary neurotrophic factor (CNTF) and CNTF-receptor alpha after spinal cord injury. Journal of Neurobiology 32:251–261. [PubMed: 9058319]

Prakash YS, Mantilla CB, Zhan WZ, Smithson KG, Sieck GC. 2000 Phrenic motoneuron morphology during rapid diaphragm muscle growth. J Appl Physiol 89:563–572. [PubMed: 10926639]

Prakash YS, Miyata H, Zhan WZ, Sieck GC. 1999 Inactivity-induced remodeling of neuromuscular junctions in rat diaphragmatic muscle. Muscle Nerve 22:307–319. [PubMed: 10086891]

Prakash YS, Smithson KG, Sieck GC. 1993 Measurements of motoneuron somal volumes using laser confocal microscopy: comparisons with shape-based stereological estimations. Neuroimage 1:95–107. [PubMed: 9343561]

Prakash YS, Smithson KG, Sieck GC. 1994 Application of the Cavalieri principle in volume estimation using laser confocal microscopy. Neuroimage 1:325–333. [PubMed: 9343582]

Satake K, Matsuyama Y, Kamiya M, Kawakami H, Iwata H, Adachi K, Kiuchi K. 2000 Up-regulation of glial cell line-derived neurotrophic factor (GDNF) following traumatic spinal cord injury. Neuroreport 11:3877–3881. [PubMed: 11117507]

Scheibel ME, Scheibel AB. 1970 Developmental relationship between spinal motoneuron dendrite bundles and patterned activity in the hind limb of cats. Exp Neurol 29:328–335. [PubMed: 4100982]

Scheibel ME, Scheibel AB. 1971 Developmental relationship between spinal motoneuron dendrites bundles and patterned activity in the forelimb of cats. Exp Neurol 30:367–373. [PubMed: 4251153]

Segal M, Andersen P. 2000 Dendritic spines shaped by synaptic activity. Current Opinion in Neurobiology 10:582–586. [PubMed: 11084320]

Sieck GC. 1995 Organization and recruitment of diaphragm motor units In: Roussos C, editor. The Thorax. Second ed. New York, NY: Marcel Dekker p 783–820.

Sieck GC, Fournier M. 1989 Diaphragm motor unit recruitment during ventilatory and nonventilatory behaviors. J Appl Physiol 66:2539–2545. [PubMed: 2745316]

Sieck GC, Prakash YS. 1997 The diaphragm muscle In: Miller AD, Bianchi AL, Bishop BP, editors. Neural Control of the Respitatory Muscles. Boca Raton, FL: CRC Press p 7–20.

Smithson KG, Cobbett P, MacVicar BA, Hatton GI. 1984 A reliable method for immunocytochemical identification of Lucifer Yellow injected, peptide-containing mammalian central neurons. J Neurosci Meth 10:59–69.

Steward O, Wallace CS, Worley PF. 2001 Synaptic plasticity in epileptogenesis: cellular mechanisms underlying long-lasting synaptic modifications that require new gene expression. Int Rev Neurobiol 45:269–292. [PubMed: 11130903]

Streeter KA, Baker-Herman TL. 2014 Decreased spinal synaptic inputs to phrenic motor neurons elicit localized inactivity-induced phrenic motor facilitation. Exp Neurol 256:46–56. [PubMed: 24681155]

Tomasulo RA, Ramirez JJ, Steward O. 1993 Synaptic inhibition regulates associative interactions between afferents during the induction of long-term potentiation and depression. Proc Natl Acad Sci U S A 90:11578–11582. [PubMed: 8265593]

Tomasulo RA, Steward O. 1996 Homosynaptic and heterosynaptic changes in driving of dentate gyrus interneurons after brief tetanic stimulation in vivo. Hippocampus 6:62–71. [PubMed: 8878744]

Trelease RB, Sieck GC, Harper RM. 1982 A new technique for acute and chronic recording of crural diaphragm EMG in cats. Electroencephalogr Clin Neurophysiol 53:459–462. [PubMed: 6175508]

Ulfhake B, Cullheim S. 1988 Postnatal development of cat hind limb motoneurons. III: Changes in size of motoneurons supplying the triceps surae muscle. J Comp Neurol 278:103–120. [PubMed: 3209749]

Widenfalk J, Lundstromer K, Jubran M, Brene S, Olson L. 2001 Neurotrophic factors and receptors in the immature and adult spinal cord after mechanical injury or kainic acid. J Neurosci 21:3457–3475. [PubMed: 11331375]

Wu J, Capelli P, Bouvier J, Goulding M, Arber S, Fortin G. 2017 A V0 core neuronal circuit for inspiration. Nat Commun 8:544. [PubMed: 28916788]

Yates BJ, Smail JA, Stocker SD, Card JP. 1999 Transneuronal tracing of neural pathways controlling activity of diaphragm motoneurons in the ferret. Neuroscience 90:1501–1513. [PubMed: 10338316]

Zhan WZ, Mantilla CB, Zhan P, Bitton A, Prakash YS, de Troyer A, Sieck GC. 2000 Regional differences in serotonergic input to canine parasternal intercostal motoneurons. J Appl Physiol 88:1581–1589. [PubMed: 10797116]

Zhan WZ, Miyata H, Prakash YS, Sieck GC. 1997 Metabolic and phenotypic adaptations of diaphragm muscle fibers with inactivation. J Appl Physiol 82:1145–1153. [PubMed: 9104851]

Zhan WZ, Sieck GC. 1992 Adaptations of diaphragm and medial gastrocnemius muscles to inactivity. J Appl Physiol 72:1445–1453. [PubMed: 1592737]

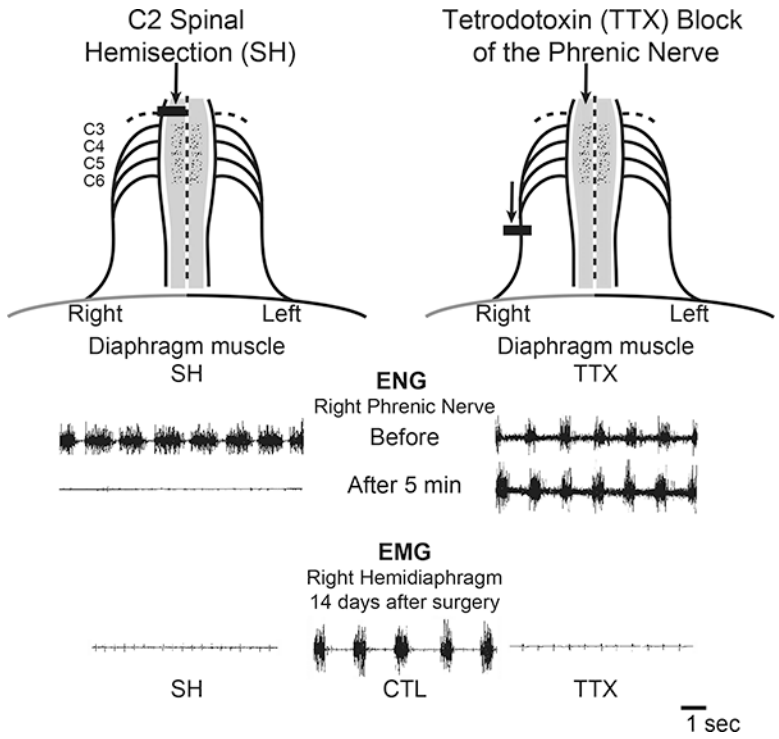

Figure 1.

Two models of diaphragm muscle paralysis were used in this study. Spinal hemisection at C2 (SH) inactivates both phrenic motoneurons and diaphragm muscle, as evidenced by the absence of ipsilateral ENG and diaphragm EMG activity. Tetrodotoxin (TTX) block of the phrenic nerve maintains phrenic motoneuron activity but inactivates the diaphragm muscle, as evidenced by the presence of ipsilateral ENG activity and lack of ipsilateral diaphragm EMG activity.

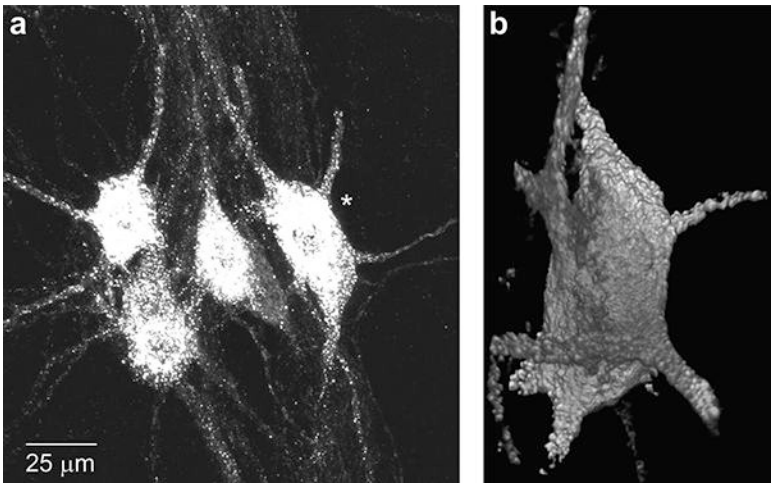

Figure 2.

Representative retrogradely-labeled phrenic motoneurons in a longitudinal section of the rat cervical spinal cord from a control animal. Note clustering of phrenic motoneurons with 3–5 motoneurons easily discerned (a). A single phrenic motoneuron (denoted by *) was sampled per cluster based on the completeness of the dendritic tree (at least 5 primary dendrites were contained in the section; b). Surface areas of motoneuron somata were estimated for a prolate spheroid by measuring the major and minor diameters of each motoneuron from the 3D reconstruction. Primary dendrites were identified and their orthogonal diameter was measured at 15 μm from the cell soma for estimates of dendritic surface area (see Methods).

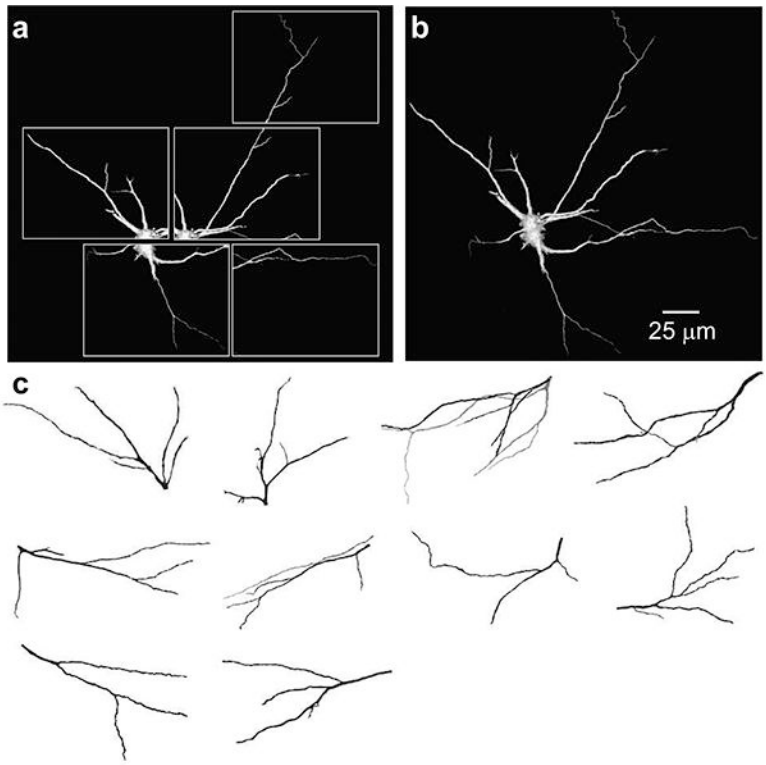

Figure 3.

Representative fuzzy-gradient volume renderings of dendritic tree objects created from optical sections of adult rat phrenic motoneurons. Separate confocal stacks of volume rendered images (a) and merged 3D image (b) from LY filled phrenic motoneurons. (c) XY view of 3D-reconstructed dendritic trees selected for analyses.

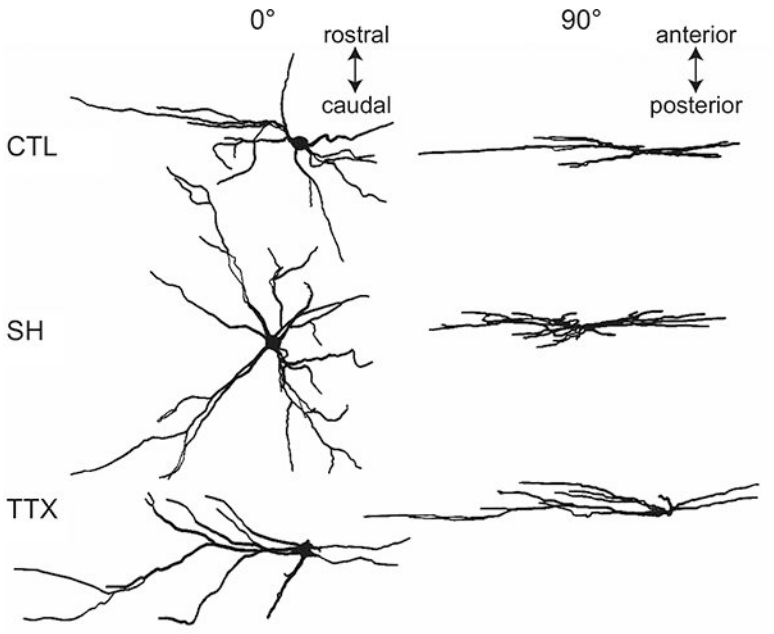

Figure 4.

Representative examples of camera lucida drawings of ipsilateral phrenic motoneuron dendritic architecture from control, C2 spinal hemisection (SH), and tetrodotoxin (TTX) nerve blockade models (shown at 0° and 90° relative to the plane of tissue section). Phrenic motoneurons were retrogradely labeled with cholera toxin subunit B (CTB).

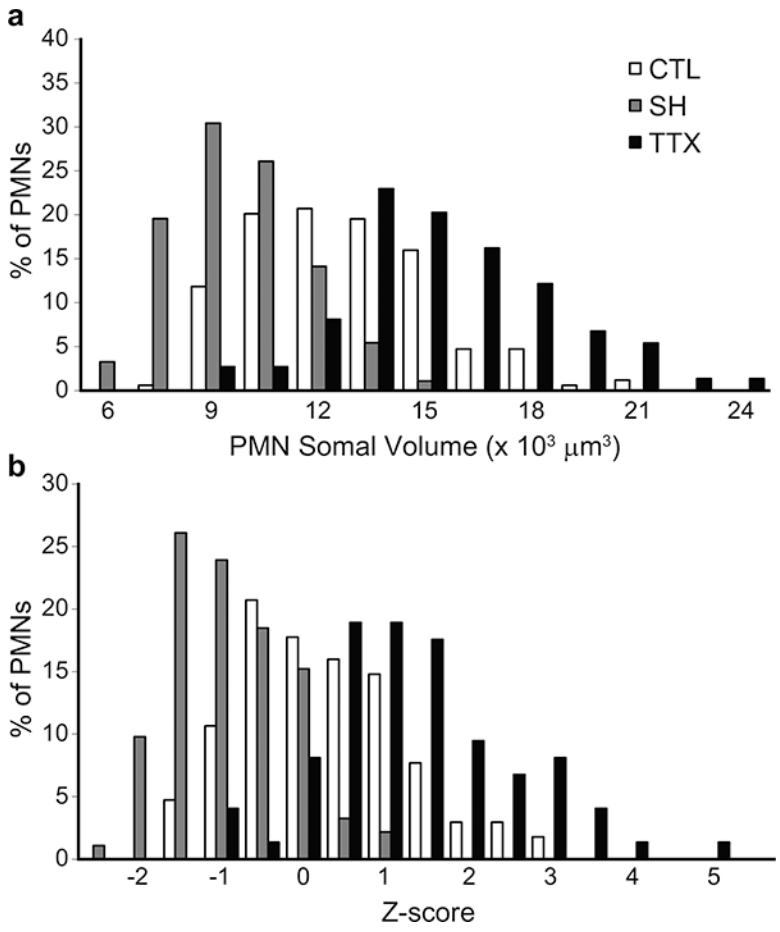

Figure 5.

Phrenic motoneuron somal volume was different across groups. (a) Distribution of phrenic motoneuron somal volumes in control, SH and TTX animals. (b) Distribution of Z-scores for the somal volumes in control, SH and TTX animals. Note the leftward shift in volume distribution with SH, indicating a decrease in the volume of larger phrenic motoneurons. In contrast, with TTX, the distribution is shifted to the right.

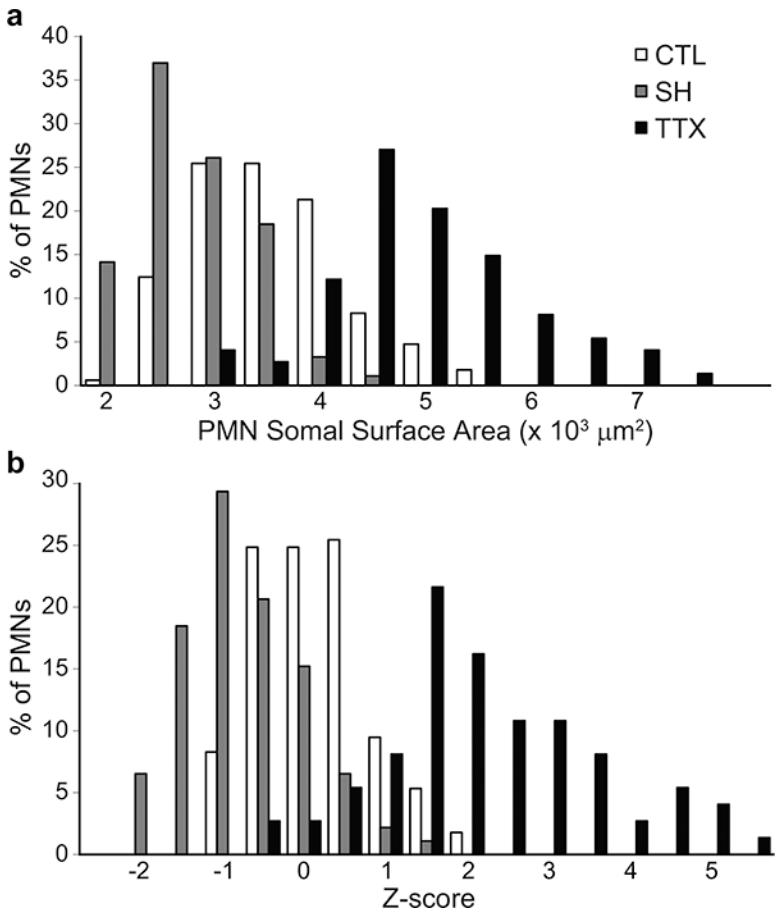

Figure 6.

Phrenic motoneuron somal surface area was different across groups. (a) Distribution of phrenic motoneuron surface areas in control, SH and TTX animals. (b) Distribution of Z-scores for somal surface areas in control, SH and TTX animals. Note the leftward shift in surface area distribution with SH, indicating a decrease in the surface area of larger phrenic motoneurons. In contrast, with TTX, the distribution is shifted to the right.

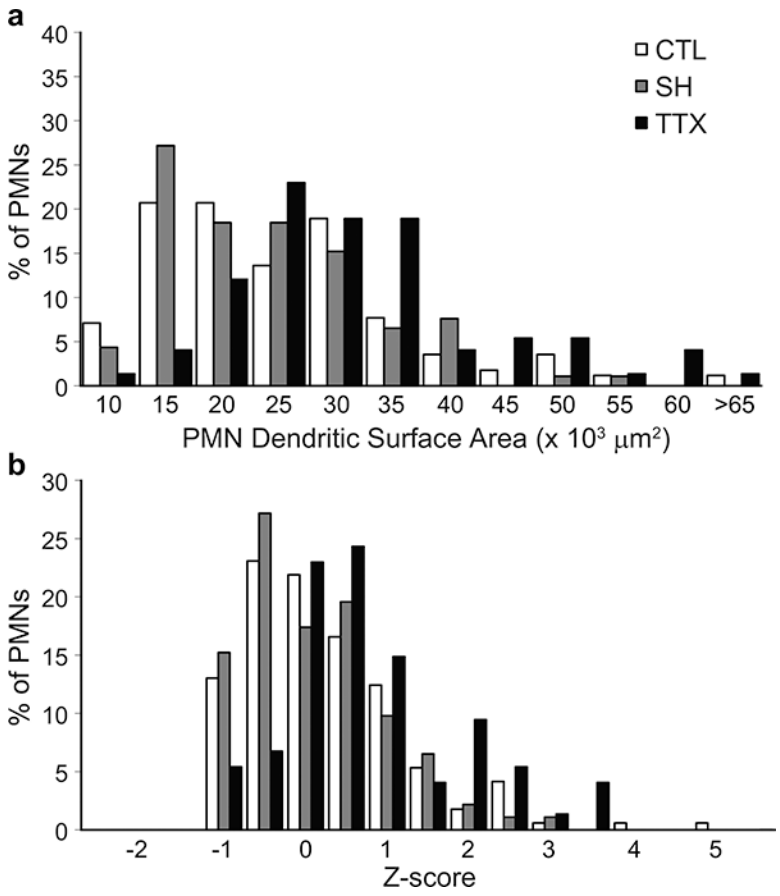

Figure 7.

Estimated phrenic motoneuron dendritic surface area was not significantly different between control and SH, but increased with TTX. (a) Distribution of phrenic motoneuron dendritic surface area in control, SH and TTX animals. (b) Distribution of Z-scores for dendritic surface areas of phrenic motoneurons in control, SH and TTX animals. Note the unchanged distribution for phrenic motoneurons in SH animals, and the significant right shift in the distribution of the TTX group.

Table 1:

Effect of spinal hemisection (SH) vs. tetrodotoxin (TTX) blockade on phrenic motoneuron dendritic morphology

Parameter	Control	SH	TTX	ANOVA p value
No. of Primary Dendrites	7.6 ± 0.1	7.3 ± 0.2	8.3 ± 0.2 *†	p=0.003
Primary Dendrite Diameter (μm)	2.4 ± 0.1	2.3 ± 0.1	2.8 ± 0.1 *†	p<0.001
Total Dendritic Length (μm)	3,748 ± 319	4,914 ± 361	4,844 ± 414	p=0.044
Average Dendritic Length (μm)	81.5 ± 4.4	69.1 ± 6.1	93.2 ± 6.7†	p=0.015
Estimated Dendritic Surface Area (μm^2)	22,722 ± 848	21,219 ± 990	29,657 ± 1,509 *†	p<0.001
Estimated Receptive Field (μm^2)	78,764 ± 5,207	99,471 ± 6,744	87,831 ± 6,942	p=0.072
Total Motoneuron Surface Area (μm^2)	26,010 ± 899	23,796 ± 1,043	34,371 ± 1,619 *†	p<0.001

Data presented are mean ± SE. SH: C2 spinal hemisection; TTX: tetrodotoxin block of the phrenic nerve.

* indicates statistical significance from control (p<0.05).

† indicates statistical significance from SH (p<0.05) after post-hoc analyses.